Journal of Alloys and Compounds 509 (2011) 6096–6101

Contents lists available at ScienceDirect

Journal of Alloys and Compounds

journal homepage: www.elsevier.com/locate/jallcom

Concentration-dependent luminescence and energy transfer of flower-like $Y_2(MoO_4)_3:Dy^{3+}$ phosphor

Yue Tian[a,b], Baojiu Chen[a,*], Bining Tian[a,b], Ruinian Hua[b,**], Jiashi Sun[a], Lihong Cheng[a], Haiyang Zhong[a], Xiangping Li[a], Jinsu Zhang[a], Yanfeng Zheng[a], Tingting Yu[a], Libo Huang[a], Qingyu Meng[c]

[a] Department of Physics, Dalian Maritime University, Dalian, Liaoning 116026, PR China
[b] College of Life Science, Dalian Nationalities University, Dalian, Liaoning 116600, PR China
[c] School of Physics and Electronic Engineering, Harbin Normal University, Harbin 150025, PR China

ARTICLE INFO

Article history:
Received 17 November 2010
Received in revised form 8 February 2011
Accepted 6 March 2011
Available online 11 March 2011

Keywords:
$Y_2(MoO_4)_3:Dy^{3+}$
Phosphor
Luminescent properties
White light emitting diodes
Energy transfer

ABSTRACT

Flower-like $Y_2(MoO_4)_3:Dy^{3+}$ phosphors have been synthesized via a co-precipitation approach with the aid of β-cyclodextrin. The crystal structure and morphology of the phosphors were characterized by XRD (X-ray diffraction) and FE-SEM (field emission scanning electron microscopy), respectively. The excitation and emission properties of the phosphors were examined by fluorescence spectroscopy. The dependence of color coordinates on the Dy^{3+} doping concentration was analyzed. The energy transfer mechanism between Dy^{3+} ions was studied based on the Huang's theory, I-H and Van Uitert's models. It was concluded simultaneously from these three routes that the electric dipole–dipole interaction between Dy^{3+} ions is the main physical mechanism for the energy transfers between Dy^{3+}.

1. Introduction

Over the past several decades, rear earth ions (RE^{3+}) doped phosphors have attracted much attention due to their potential applications in plasma display panels (PDPs), field emission displays (FEDs), fluorescent lamps and so on [1–15]. In recent years, with the technical mature of GaN-based LEDs, it is possible to achieve solid state illumination by combining short wavelength GaN-based LED chips with tricolor phosphors. However, the tricolor phosphors for this application are of lack. The presently commercialized W-LEDs are a combination of blue GaN-based LED chip with yellow-emitting YAG:Ce^{3+} phosphor, which shows poor color rendering index and is unsatisfactory for the high performance illumination [16]. Generally, trivalent dysprosium (Dy^{3+}) ion has two intense emission bands in the blue (470–500 nm) and yellow (560–600 nm) regions [17]. The yellow emission ($^4F_{9/2} \rightarrow {}^6H_{13/2}$) is an electric dipole transition, which is very sensitive to the crystal field. The blue emission ($^4F_{9/2} \rightarrow {}^6H_{15/2}$) is a magnetic dipole transition, which is insensitive to the crystal field. Therefore, it is possible to obtain white light from Dy^{3+} activated luminescent materials by adjusting the intensity ratio of yellow to blue emissions (Y/B) via choosing different hosts [18].

Molybdates are important inorganic compounds and have exhibited some excellent performance in the fields of catalysts, lasers and ionic conductors [19–21]. Recently, RE^{3+} doped molybdates are also studied widely on the purpose of seeking for novel luminescence materials for W-LEDs due to the special properties of MoO_4^{2-} group [4,22–24]. As well known, MoO_4^{2-} group has strong absorption in the near UV region. Therefore, the energy transfer process from MoO_4^{2-} group to RE^{3+} can easily occur, which can greatly enhance the external quantum efficiency of RE^{3+} doped materials. However, as far as we know, there is no report on Dy^{3+} doped $Y_2(MoO_4)_3$ phosphor. In this paper, we prepared $Y_2(MoO_4)_3$ phosphors with various Dy^{3+} concentrations via a co-precipitation process with the aid of β-cyclodextrin. The prepared $Y_2(MoO_4)_3:Dy^{3+}$ samples showed uniform flower shaped and porous structure. The characteristic emissions of Dy^{3+} in $Y_2(MoO_4)_3$ phosphors were observed under UV light excitation. The energy transfer mechanism between Dy^{3+} ions in the $Y_2(MoO_4)_3$ phosphors was discussed based on the analysis of concentration quenching and fluorescent dynamics.

2. Experimental

2.1. Sample synthesis

All reagents used in this work are analytical grade without any further purification except for the spectrographically pure Dy_2O_3 and Y_2O_3. $Dy(NO_3)_3{\cdot}6H_2O$ and $Y(NO_3)_3{\cdot}6H_2O$ were prepared through dissolving Dy_2O_3 and Y_2O_3 in nitric acid (the volume ratio between nitric acid and water is 1:1). Then, the resultant solutions were

* Corresponding author. Tel.: +86 411 84728909; fax: +86 411 84728909.
** Corresponding author. Tel.: +86 411 87633470.
E-mail addresses: chenmbj@sohu.com (B. Chen), rnhua@dlnu.edu.cn (R. Hua).

0925-8388/$ – see front matter © 2011 Elsevier B.V. All rights reserved.
doi:10.1016/j.jallcom.2011.03.034

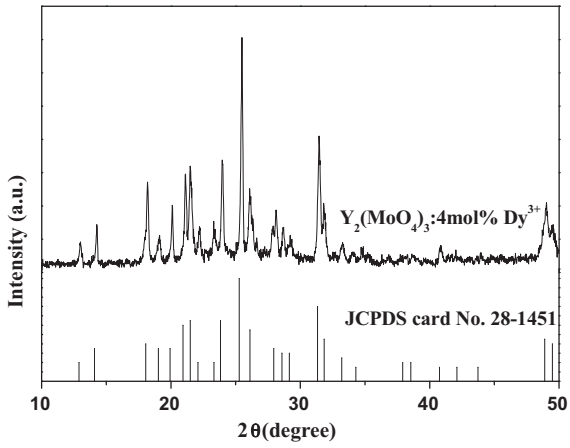

Fig. 1. XRD patterns for the studied $Y_2(MoO_4)_3$:4 mol% Dy^{3+} phosphor and for crystal $Y_2(MoO_4)_3$ reported in JPCDS card No. 28-1451.

re-crystallized three times. Lastly, the $Dy(NO_3)_3{\cdot}6H_2O$ and $Y(NO_3)_3{\cdot}6H_2O$ powders were obtained when the corresponding solutions were well dried in air at 90 °C for 12 h.

A series of $Y_2(MoO_4)_3$ phosphor with different Dy^{3+} concentrations were synthesized via a simple co-precipitation method with the aid of β-cyclodextrin. A typical synthesis procedure is described as follows. Firstly, 0.2 g of β-cyclodextrin was dissolved in 50 mL of distilled water under vigorous magnetic stirring. After β-cyclodextrin was completely dissolved, 10 mL of $Y(NO_3)_3$ and $Dy(NO_3)_3$ aqueous solution, which contain 0.002 mol (0.7662 g) of $Y(NO_3)_3{\cdot}6H_2O$, and 4×10^{-5} mol (0.0178 g, 4.0 mol% of Dy^{3+}) of $Dy(NO_3)_3{\cdot}6H_2O$, was poured into β-cyclodextrin aqueous solution under vigorous magnetic stirring. Then, 10 mL of Na_2MoO_4 aqueous solution (3 mol/L) was slowly dropped into the above solution under magnetic stirring, and the white precipitation was formed immediately. After reacting for 0.5 h, the product was collected by centrifugation at 4500 rpm for 10 min. The resultant white precipitate was washed three times with distilled water, and then dried at 80 °C in air for 12 h. Finally, the $Y_2(MoO_4)_3$:Dy^{3+} phosphor was obtained after the resultant precursor was calcined at 900 °C for 1 h.

2.2. Sample characterization

The crystal structure of the samples were examined by means of XRD performed on an XRD-6000 (Shimadzu, Japan) diffractometer by using Cu $K\alpha_1$ radiation (λ = 0.15406 nm). The XRD data were collected by using a scanning mode in the 2θ range from 10° to 50° with a scanning step of 0.02° and a scanning rate of 4.0° min^{-1}. Silicon was used as an internal standard. FE-SEM images were obtained using a Hitachi S-4800 field emission scanning electron microscopy operating at acceleration voltage of 3 kV. Photoluminescence (PL) emission and excitation spectra were recorded with a Hitachi F-4600 spectrophotometer equipped with a 150 W xenon lamp as an excitation source. All measurements were carried out at room temperature.

3. Results and discussion

3.1. Crystal structure and morphology of Dy^{3+} doped $Y_2(MoO_4)_3$ phosphor

The crystal structure for all the prepared Dy^{3+} doped $Y_2(MoO_4)_3$ phosphors was checked by XRD. All the samples displayed the same diffraction pattern. Fig. 1 shows an example of the XRD pattern for the $Y_2(MoO_4)_3$ phosphor doped with 4 mol% Dy^{3+}. The bottom part of Fig. 1 lays out the diffraction pattern for the $Y_2(MoO_4)_3$ crystal reported in the JPCDS card No. 28-1451. It can be found that the positions of all the diffraction peaks for the studied sample are in good agreements with those appearing in the standard JCPDS card No. 28-1451. There no such diffraction peaks belonging to other impurity phase were observed, thus indicating that the samples studied in this work are single phase.

The SEM images for all the samples with different Dy^{3+} concentrations were taken, and that all of them exhibit the same morphology. This fact means that Dy^{3+} doping does not influence the shape and size of the resultant phosphors at the present

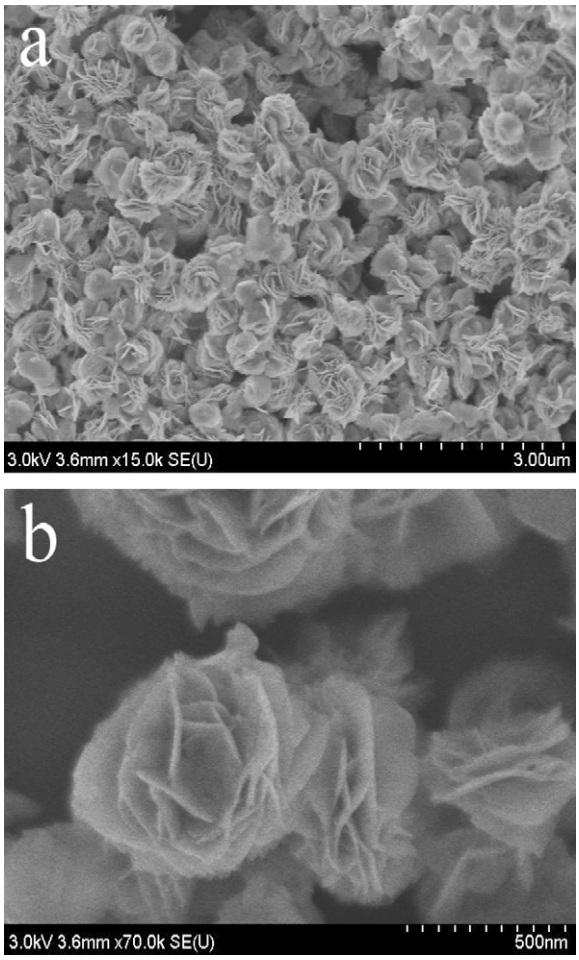

Fig. 2. FE-SEM images of $Y_2(MoO_4)_3$: 4 mol% Dy^{3+} phosphor. (a) low and (b) high magnification.

doping level. As an example, the low and high magnification FE-SEM images for the sample mentioned in Fig. 1 are exhibited in Fig. 2(a) and (b). It can be seen clearly from these images that the $Y_2(MoO_4)_3$:Dy^{3+} sample exhibits flower-like shape with an average gain size of about 600 nm. Moreover, every flower-shaped particle is buit by many nanoflakes with the thickness of around 20 nm. The flakes intercross with each other to form a porous flower-shaped structure. It is worthwhile to mention that in our previous work [4] the flower shaped $Y_2(MoO_4)_3$:Eu^{3+} phosphors prepared via co-precipitation method without the aid of β-cyclodextrin exhibited nonuniform morphology and size. This fact tells us that the addition of β-cyclodextrin is beneficial to the growth of the flower-shaped particles.

3.2. Emission properties of $Y_2(MoO_4)_3$:Dy^{3+} phosphor

Fig. 3 depicts the emission spectra of $Y_2(MoO_4)_3$:x mol% Dy^{3+} (x = 0.5–10) phosphors excited at 388 nm. The emission spectra display two main peaks in the blue (460–500 nm) and yellow (555–610 nm) regions as well as a weak line in the red region. These blue, yellow and red emissions can be attributed to the electronic transitions of $^4F_{9/2} \rightarrow {}^6H_{15/2}$, $^4F_{9/2} \rightarrow {}^6H_{13/2}$ and $^4F_{9/2} \rightarrow {}^6H_{11/2}$, respectively [17]. The blue emission is natured of magnetic dipole transition, and the yellow emission belongs to the hypersensitive (forced electric dipole) transition following the selection rule, $\Delta J = 2$. In the studied $Y_2(MoO_4)_3$:Dy^{3+} phosphors, the integrated intensity of yellow emission is greater than that of the blue emission. It is well known that the hypersensitive

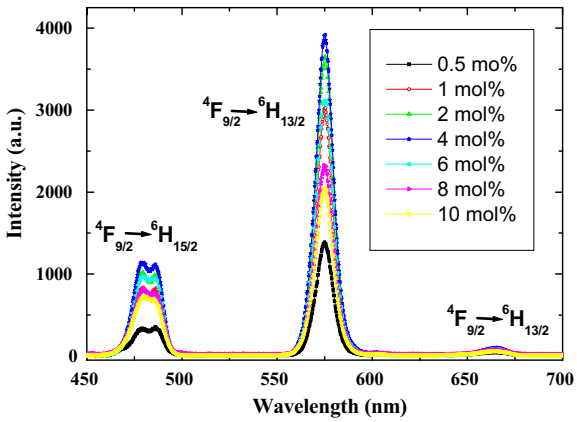

Fig. 3. Emission spectra for the $Y_2(MoO_4)_3$ phosphors with different doping concentrations of Dy^{3+} under 388 nm excitation.

transition is strongly influenced by the outside environment surrounding Dy^{3+}, and the magnetic dipole transition is insensitive to the crystal field around the Dy^{3+} ions. When Dy^{3+} is located at a low symmetry site (without inversion symmetry), the yellow emission is dominant in the emission spectrum; when Dy^{3+} is at a high symmetry site (with inversion symmetry), the blue emission would be stronger than the yellow one [18,25]. Thus, the stronger yellow emission indicates that Dy^{3+} ions take the site without inversion symmetry. In addition, it can also be found that with increase of Dy^{3+} ions concentration, the intensities of both blue and yellow emissions increase firstly and reach their maximums at 4 mol%, and then decrease, namely, fluorescence quenching happens. The fluorescence quenching behavior can be explained by the cross relaxations between Dy^{3+} ions. There are at least 3 possible cross relaxation channels responsible for the population decrease of $^4F_{9/2}$ level: $^4F_{9/2} + {}^6H_{15/2} \rightarrow {}^6F_{9/2}/{}^6H_{7/2} + {}^6F_{3/2}$, $^4F_{9/2} + {}^6H_{15/2} \rightarrow {}^6H_{9/2}/{}^6F_{11/2} + {}^6F_{5/2}$ and $^4F_{9/2} + {}^6H_{15/2} \rightarrow {}^6F_{1/2} + {}^6H_{9/2}/{}^6H_{11/2}$ [26].

By carefully inspecting the emission spectra of the samples with various Dy^{3+} concentrations, it can be found that the integrated emission intensity ratio of yellow to blue (Y/B) changes with Dy^{3+} doping concentration. The dependence of the Y/B ratio on Dy^{3+} doping concentration in $Y_2(MoO_4)_3$ phosphors is depicted in Fig. 4. The solid squares show the experimental data, and the solid line indicates the variation trend. It can be seen that the integrated intensity ratio for each sample ranges from 1.9 to 2.5. The change of the ratio

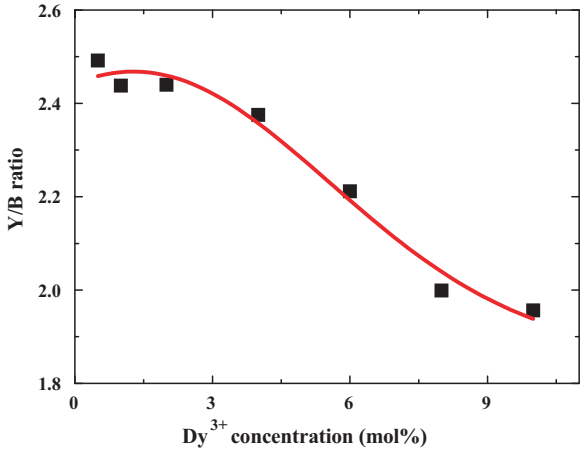

Fig. 4. Dependence of Y/B ratio on Dy^{3+} doping concentration in $Y_2(MoO_4)_3$ phosphors. Squared dots present the experimental data, solid line shows the variation trend.

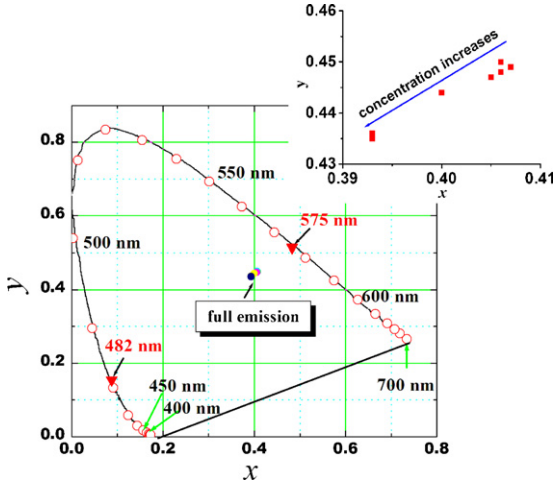

Fig. 5. CIE color coordinates for the $Y_2(MoO_4)_3$ phosphors with various Dy^{3+} concentrations, the triangle dots show the color coordinates for solo- blue and yellow emission, solid circle dots for the full emissions, the insert at the top-right corner shows the color coordinates of the phosphor in the part of color space. (For interpretation of the references to color in this figure legend, the reader is referred to the web version of the article.)

is probably due to the fact that with increasing Dy^{3+} concentration the covalency degree of Dy^{3+}–O^{2-} bond would decrease, thus Y/B ratio decreases [27]. It should be noted that for all the samples with different Dy^{3+} concentrations the yellow integrated emission intensity is still higher than the blue one, which means that Dy^{3+} ions still occupy the site without inversion symmetry [25].

3.3. Colorimetric characterization

Color coordinates are one of the important factors for evaluating the performance of phosphors. In this work, the color coordinates for all the samples with various Dy^{3+} concentrations were calculated using the intensity-calibrated emission spectra data and the chromatic standard issued by the Commission International de l'Eclairage (CIE) in 1931 (CIE 1931), since the samples with different Dy^{3+} concentrations exhibit different spectral profiles (Y/B ratio changes). Fig. 5 shows the obtained color coordinates for full emissions of the samples doped with x mol% Dy^{3+} (x = 0.5–10). The insert at the top-right corner of Fig. 5 displays the magnified plot for the color coordinates in a part of the color space. It is found that with the increase of Dy^{3+} concentration, the color coordinates change from (0.407, 0.449) to (0.393, 0.435). In addition, the color coordinates for solo yellow (575 nm) and solo blue (482 nm) emissions were also calculated and shown in Fig. 5 as solid triangle dots. It can be seen that the straight line connecting the color coordinates points of blue and yellow emissions in the chromatic space just crosses the white light region, which means that the white light can be formed by mixing these two emissions. However, the calculated color coordinates for full emissions are a little far from the equal energy point (x = 0.333, y = 0.333), thus indicating that the relative intensity of blue emission is weak for forming high quality white light. In order to further improve the CIE color coordinates and achieve good quality white light, some other dopants emitting blue may need to be introduced into this phosphor system, for instance Tm^{3+}.

3.4. Excitation properties of $Y_2(MoO_4)_3$:Dy^{3+} phosphor

Fig. 6 shows the excitation spectra for all the $Y_2(MoO_4)_3$ phosphors with different Dy^{3+} concentrations while monitoring 575 nm emission corresponding to the $^4F_{9/2} \rightarrow {}^6H_{13/2}$ transition of Dy^{3+}. All

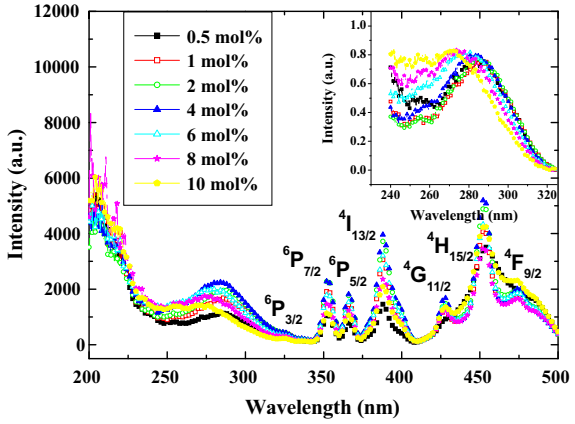

Fig. 6. Excitation spectra of $Y_2(MoO_4)_3$:Dy^{3+} phosphors with different concentrations of Dy^{3+}, monitoring at 575 nm. Insert is dependence of the host absorption band on Dy^{3+} concentration.

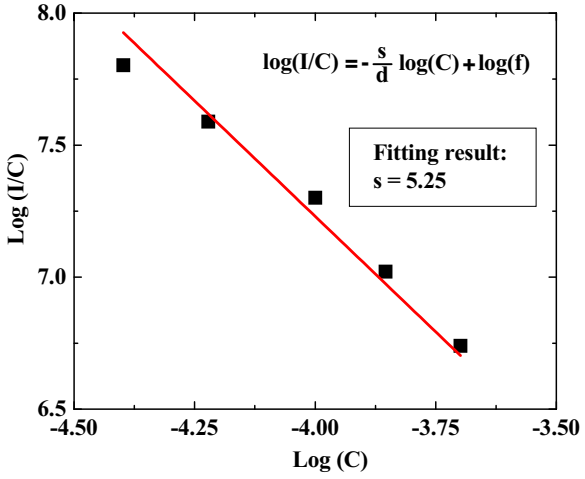

Fig. 7. Plot of $\log(I/C)$ versus $(\log C)$ for $^4F_{9/2} \rightarrow {}^6H_{13/2}$ transition of Dy^{3+} in $Y_2(MoO_4)_3$ phosphors. The squared dots show the experimental data, solid line is the fitting curve based on Huang's model.

excitation spectra are composed of two parts. One is a broad band ranging from 250 to 350 nm, which is attributed to the absorption band of MoO_4^{2-} group. The existence of host absorption band in the excitation spectrum suggests that the energy transfer from MoO_4^{2-} group to Dy^{3+} occurs. The other part is composed of some sharp lines located at 328, 353, 366, 388, 428, 452, and 475 nm. These sharp lines are due to the f–f transitions of Dy^{3+} ion from ground state $^6H_{15/2}$ to upper states $^6P_{3/2}$, $^6P_{7/2}$, $^6P_{5/2}$, $^4I_{13/2}$ $^4G_{11/2}$, $^4H_{15/2}$ and $^4F_{9/2}$ [28]. It should be mentioned that the central position of absorption band of MoO_4^{2-} group depends on the Dy^{3+} doping concentration as seen in the insert of Fig. 6. The central position of MoO_4^{2-} absorption band shifts to higher energy side when Dy^{3+} doping concentration is more than 6 mol%. Generally, the energy of CTB (charge transfer band) is closely related with the degree of covalency of metal–O ligand (M–O) bond, and the Dy^{3+} introduction makes degree of covalency increase [29]. The stronger the degree of covalency of M–O bond, the greater the CTB energy is. This is because of that the electrons are very difficult to be transferred from O^{2-} orbital to the Mo^{n+} ion at the strong degree of covalency of M–O bond. Thus, the introduction of Dy^{3+} leads to the blue-shift of CTB. This result also implies that the Dy^{3+} doping changes the local environment surrounding Dy^{3+} and consequently evokes CTB variation.

3.5. Energy transfer between Dy^{3+} ions in $Y_2(MoO_4)_3$:Dy^{3+} phosphor

Energy transfer behavior is widely existent in the RE doped luminescence materials. The nature of an energy transfer is decided by the microscopic physical mechanisms of the interactions between luminescent centers. Indubitably, comprehensive understanding to the energy transfer process is helpful to the design of luminescence materials. Huang and his coworker have started from the fundamental theory of energy transfer and developed a theoretical description for the relationship between the luminescent intensity and the doping concentration [30]. With Huang's description the interaction mechanism between doping centers can be recognized via inspection of concentration quenching. Our previous results have examined Huang's theoretical description [4,31], and good agreements were achieved. According to Huang's results, the relationship between luminescent intensity I and doping concentration C could be expressed as following,

$$I \propto a^{(1-s/d)}\Gamma\left(1+\frac{s}{d}\right) \quad (1)$$

$$a = C\Gamma\left(1-\frac{d}{s}\right)\left[X_0\left(1+\frac{A}{\gamma}\right)\right]^{d/s} \quad (2)$$

where γ is the intrinsic transition probability of donor, s is index of electric multipole. For electric dipole–dipole, electric dipole–quadrupole and electric quadrupole–quadrupole interactions, s equals to 6, 8 and 10, respectively. d is dimension of the sample, here $d = 3$ since the energy transfer between Dy^{3+} ions happens inside the particles, A and X_0 are constant, $\Gamma(1+s/d)$ is Γ function. From Eqs. (1) and (2) it can be derived that:

$$\log\left(\frac{I}{C}\right) = -\frac{s}{d}\log\ C + \log f \quad (3)$$

where f is independent from the doping concentration.

Fig. 7 shows the $\log(I/C) - \log(C)$ plot for the $^4F_{9/2} \rightarrow {}^6H_{13/2}$ transition of Dy^{3+} ions in the $Y_2(MoO_4)_3$:Dy^{3+} phosphor. According to Eq. (3), using linear fittings to deal with the experimental data in the region of high Dy^{3+} concentration, the value of the slope parameter s/d can be derived to be 1.75, corresponding to $s = 5.25$, which is close to 6. This means that the electric dipole–dipole interaction is responsible for the energy transfer between Dy^{3+} ions in the $Y_2(MoO_4)_3$:Dy^{3+} phosphors.

In order to further study on the energy transfer behavior, the fluorescent decay for 0.5 mol% Dy^{3+} doped $Y_2(MoO_4)_3$ phosphor

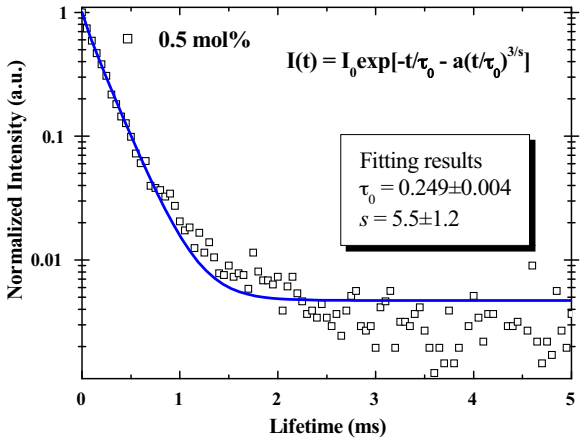

Fig. 8. Squared dots show the measured fluorescent decay of $Y_2(MO_4)_3$ phosphor with 0.5 mol% Dy^{3+} ions ($\lambda_{ex} = 388$ nm, $\lambda_{em} = 575$ nm). Solid line shows the fitting curve by using I-H model.

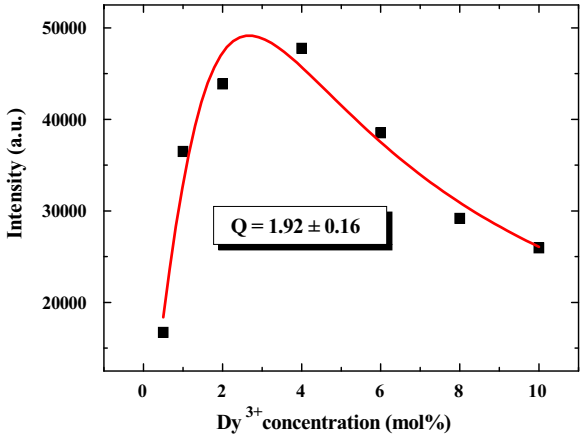

Fig. 9. Dependence of yellow emission intensity on Dy^{3+} concentration in $Y_2(MoO_4)_3$:Dy^{3+} phosphors. Solid line is the fitting curve by using Van Uitert's model.

was measured by monitoring 577 nm emission, while excited with 388 nm pulsed light. The fluorescent decay curve is shown in Fig. 8, where the open-squared dots are the experimental data. It can be seen that the decay curve show non-exponential dependence of emission intensity on the decay time even at this low doping concentration. Inokuti and Hirayama have established a model to explain the non-exponential behavior of fluorescence decay, which so called I-H model [32]. In this model the intensity $I(t)$ can be expressed as follows:

$$I(t) = I_0 \exp\left[-\frac{t}{\tau_0} - \alpha\left(\frac{t}{\tau_0}\right)^{3/s}\right] \quad (4)$$

where $I(t)$ is the luminescence intensity at time t, I_0 is the luminescence intensity at $t = 0$ and τ_0 is the intrinsic lifetime of the donor. s has the same meaning as in Eq. (3). α is a parameter containing energy transfer probability. According to Eq. (4), using nonlinear fittings to deal with the experimental data, the fitting results are shown in Fig. 8. In the fitting process, the s is confirmed to be 5.5, which approximates 6. This result is in accordance with that derived from Huang's theory. In addition, the intrinsic radiative transition lifetime τ_0 of $^4F_{9/2}$ level of Dy^{3+} is also confirmed in the fitting process to be 0.249 ms.

Van Uitert has developed a phenomenological description with regard to the dependence of donor emission intensity on the doping concentration based on different physical consideration from Huang's model. In Van Uitert's model the relationship between the luminescent intensity and the doping concentration can be expressed as below [33,34]:

$$I(C) = \frac{C}{K(1 + \beta C^{Q/3})} \quad (5)$$

where C is concentration of donor, K and β are constants for a certain system, Q represents the interaction type between donors, here $Q = 3$, 6, 8 or 10, indicating the exchange interaction, electric dipole–dipole, electric dipole–quadrupole, or electric quadrupole–quadrupole interactions, respectively. A nonlinear fitting by using Eq. (5) was carried out on the concentration quenching data shown in Fig. 9.It can be seen that the optimum concentration for obtaining maximum luminescent intensity is 4 mol%. The $Q/3$ value was confirmed from this fitting process to be 1.92, which means that Q is approximately 6. That is to say that the electric dipole–dipole interaction between Dy^{3+} ions is the main mechanism for the luminescence quenching of Dy^{3+} ions in $Y_2(MoO_4)_3$ phosphor. From above discussion, it can be concluded that the I-H model, Huang's theory and Van Uitert's model can well explain the physical mechanisms for the interaction between rare earth ions.

4. Conclusion

$Y_2(MoO_4)_3$:Dy^{3+} phosphors were synthesized via a facile co-precipitation route with the aid of β-cyclodextrin. The XRD revealed that the products with various Dy^{3+} concentrations are composed of mono-phase $Y_2(MoO_4)_3$. FE-SEM results proved that the phosphor particles display flower-like shape, which is composed of some nanoflakes with the thickness about 20 nm. Under 388 nm excitation, the $Y_2(MoO_4)_3$:Dy^{3+} phosphors exhibit the characteristic emissions of Dy^{3+}. The optimum doping concentration of Dy^{3+} ions was confirmed to be 4 mol%. The blue shift of charge transfer band and decrease of Y/B ratio were observed with the increase of Dy^{3+} ions concentration, which indicates that the introduction of Dy^{3+} leads to the change of covalency degree of Dy^{3+}–O^{2-}–Mo^{6+} bond. The color coordinates for the Dy^{3+} doped $Y_2(MoO_4)_3$ phosphors were calculated. Electric dipole–dipole interaction is dominant mechanism for energy transfer between Dy^{3+} ions in the $Y_2(MoO_4)_3$:Dy^{3+} phosphors. The intrinsic fluorescent lifetime of $^4F_{9/2}$ level is concluded to 0.249 ms.

Acknowledgments

This work was partially supported by NSFC (National Natural Science Foundation of China, grant no. 50972021, 61078061 and 51002041), Natural Science Foundation of Liaoning Province (grant no. 20092147), Foundation of Education Department of Liaoning Province (grant no. L2010056 and L2010057), Fundamental Research Funds for the Central Universities (grant no. 2009QN066, 017125 and DC10020105) and Technology Services Pre-research Project Fund of Dalian Nationalities University (2009B301).

References

[1] R.M. Martinez, A.C. Ira, A. Speghini, C. Falcony, U. Caldino, J. Alloys Compd. 509 (2011) 3160.
[2] Godbole, H.C. Swart, J. Alloys Compd. 509 (2011) 2544.
[3] Y. Tian, B.J. Chen, R.N. Hua, L.H. Cheng, H.Y. Zhong, J.S. Sun, B. Wang, J. Wan, W.L. Lu, K. Jang, J. Nanosci. Nanotechnol. 10 (2010) 1943.
[4] Y. Tian, X.H. Qi, X.W. Wu, R.N. Hua, B.J. Chen, J. Phys. Chem. C 113 (2009) 10767.
[5] C.H. Huang, T.W. Kuo, T.M. Chen, ACS Appl. Mater. Interfaces 2 (2010) 1395.
[6] Q. Li, J. Huang, D. Chen, J. Alloys Compd. 509 (2011) 1007.
[7] W.H. Di, X.J. Wang, B.J. Chen, H.S. Lai, X.X. Zhao, Opt. Mater. 27 (2005) 1386.
[8] H. He, X. Song, R. Fu, Z. Pan, X. Zhao, Z. Deng, Y. Cao, J. Alloys Compd. 493 (2010) 401.
[9] B. Yan, F. Lei, J. Alloys Compd. 507 (2010) 460.
[10] I.M. Nagpure, S.J. Dhoble, M. Mohapatra, V. Kumar, S.S. Pitale, O.M. Ntwaeaborwa, S.V. Godbole, H.C. Swart, J. Alloys Compd. 509 (2011) 2544.
[11] X.M. Liu, J. Lin, Solid State Sci. 11 (2009) 2030.
[12] T. Yu, J. Sun, R. Hua, L. Cheng, H. Zhong, X. Li, H. Yu, B. Chen, J. Alloys Compd. 509 (2011) 391.
[13] X. Qu, L. Cao, W. Liu, G. Su, C. Xu, P. Wang, J. Alloys Compd. 494 (2010) 196.
[14] Y. Shi, Y. Wang, Z. Yang, J. Alloys Compd. 509 (2011) 3128.
[15] Z. Sun, Q. Zhang, Y. Li, H. Wang, J. Alloys Compd. 506 (2010) 338.
[16] S. Neeraj, N. Kijima, A.K. Cheetham, Chem. Phys. Lett. 387 (2004) 2.
[17] M. Jayasimhadri, B.V. Ratnam, K. Jang, H.S. Lee, B.J. Chen, S.S. Yi, J.H. Jeong, L.R. Moorthy, J. Am. Ceram. Soc. 93 (2010) 494.
[18] Q. Su, J. Lin, B. Li, J. Alloys Compd. 225 (1995) 120.
[19] W.X. Kuang, Y.N. Fan, K.W. Yao, Y. Chen, J. Solid State Chem. 140 (1998) 354.
[20] E. Sani, A. Toncelli, M. Tonelli, D.A. Lis, E.V. Zharikov, K.A. Subbotin, V.A. Smirnov, J. Appl. Phys. 97 (2005) 123531.
[21] D. Marrero-Lopez, P. Nunez, M. Abril, V. Lavin, U.R. Rodriguez-Mendoza, V.D. Rodriguez, J. Non-Cryst. Solids 345–346 (2004) 377.
[22] Z.L. Wang, H.B. Liang, L.Y. Zhou, J. Wang, M.L. Gong, Q. Su, J. Lumin. 128 (2008) 147.
[23] X.X. Zhao, X.J. Wang, B.J. Chen, Q.Y. Meng, B. Yan, W.H. Di, Opt. Mater. 29 (2007) 1680.
[24] J. Wan, L.H. Cheng, J.S. Sun, H.Y. Zhong, X.P. Li, W.L. Lu, Y. Tian, H. Lin, B.J. Chen, J. Alloys Compd. 496 (2010) 331.
[25] M. Yu, J. Lin, Z. Wang, J. Fu, S. Wang, H.J. Hang, Y.C. Han, Chem. Mater. 14 (2002) 2224.
[26] L.H. Cheng, X.P. Li, J.S. Sun, H.Y. Zhong, Y. Tian, J. Wan, W.L. Lu, Y.F. Zheng, T.T. Yu, L.B. Huang, H.Q. Yu, B.J. Chen, Phys. B: Condens. Matter 405 (2010) 4457.
[27] Q. Su, Z.W. Pei, L.S. Chi, H.J. Zhang, Z.Y. Zhang, F. Zou, J. Alloys Compd. 192 (1993) 25.

[28] G.S. Rama Raju, J.Y. Park, H.C. Jung, H.K. Yang, B.K. Moon, J.H. Jeong, J.H. Kim, Opt. Mater. 31 (2009) 1210.
[29] Z.W. Pei, Q. Su, S.H. Li, J. Lumin. 50 (1991) 123.
[30] S.H. Huang, L.R. Lou, Chin. J. Lumin. 11 (1990) 1.
[31] Q.Y. Meng, B.J. Chen, W. Xu, Y.M. Yang, X.X. Zhao, W.H. Di, S.Z. Lu, X.J. Wang, J.S. Sun, L.H. Cheng, T. Yu, Y. Peng, J. Appl. Phys. 102 (2007) 093505.
[32] M. Inokuti, F. Hirayama, J. Chem. Phys. 43 (1965) 1978.
[33] L.G. Van Uitert, J. Electrochem. Soc. 114 (1967) 1048.
[34] Y. Tian, B.J. Chen, R.N. Hua, H.Y. Zhong, L.H. Cheng, J.S. Sun, W.L. Lu, J. Wan, Phys. B: Condens. Matter 404 (2009) 3598.